Environ Geol (2008) 54:1667–1675
DOI 10.1007/s00254-007-0948-7

ORIGINAL ARTICLE

Seal integrity and feasibility of CO_2 sequestration in the Teapot Dome EOR pilot: geomechanical site characterization

Laura Chiaramonte · Mark D. Zoback · Julio Friedmann · Vicki Stamp

Received: 9 June 2006 / Accepted: 29 November 2006 / Published online: 27 July 2007

Abstract This paper reports a preliminary investigation of CO_2 sequestration and seal integrity at Teapot Dome oil field, Wyoming, USA, with the objective of predicting the potential risk of CO_2 leakage along reservoir-bounding faults. CO_2 injection into reservoirs creates anomalously high pore pressure at the top of the reservoir that could potentially hydraulically fracture the caprock or trigger slip on reservoir-bounding faults. The Tensleep Formation, a Pennsylvanian age eolian sandstone is evaluated as the target horizon for a pilot CO_2 EOR-carbon storage experiment, in a three-way closure trap against a bounding fault, termed the S1 fault. A preliminary geomechanical model of the Tensleep Formation has been developed to evaluate the potential for CO_2 injection inducing slip on the S1 fault and thus threatening seal integrity. Uncertainties in the stress tensor and fault geometry have been incorporated into the analysis using Monte Carlo simulation. The authors find that even the most pessimistic risk scenario would require $\sim$10 MPa of excess pressure to cause the S1 fault to reactivate and provide a potential leakage pathway. This would correspond to a CO_2 column height of $\sim$1,500 m, whereas the structural closure of the Tensleep Formation in the pilot injection area does not exceed 100 m. It is therefore apparent that CO_2 injection is not likely to compromise the S1 fault stability. Better constraint of the least principal stress is needed to establish a more reliable estimate of the maximum reservoir pressure required to hydrofracture the caprock.

Keywords CO_2 · Geomechanics · Natural leakage · Fault stability · Seal integrity

L. Chiaramonte (✉) · M. D. Zoback
Geophysics Department, Stanford University,
397 Panama Mall, Room 360,
Stanford, CA 94305-2215, USA
e-mail: chiarlau@pangea.stanford.edu

J. Friedmann
Lawrence Livermore National Laboratory,
7000 East Avenue, Livermore, CA 94550-9234, USA

V. Stamp
Rocky Mountain Oilfield Testing Center (RMOTC),
907 N. Poplar, Suite 150, Casper, WY 82601, USA

Introduction

One of the main issues to be addressed for CO_2 sequestration to be a viable carbon management solution is the risk of CO_2 leakage. From a technical perspective, depleted or mature oil and gas reservoirs hold great promise as sequestration sites due to the fact that hydrocarbons were held in them for geological periods of time, implying the presence of effective trap and seal mechanisms. However, it has long been known (e.g., Raleigh et al. 1976) that fluid injection causes changes in the pore pressure and stress field that could potentially alter the initial seal of the reservoir by either hydraulically fracturing the cap rock or by triggering slip on pre-existing faults by reducing the effective normal stress on the fault plane (see review by Grasso 1992).

In light of this, one of the key steps in the evaluation of any potential site being considered for geologic carbon sequestration is the ability to predict whether the increased pressures associated with CO_2 sequestration are likely to affect seal capacity. Although it has been recognized that one possible leakage route in depleted oil and gas fields may be the damaged casings of old or abandoned wells, the focus of the present work is to evaluate the potential risk of CO_2 leakage through natural pathways by inducing slip on faults that are currently sealing and bounding the hydrocarbon reservoirs.

It is thus essential to study the relationship between faults and the present-day stress field to predict which faults could be potential leakage routes. Another way of compromising seal integrity is by hydrofracturing the cap rock, which occurs when the pore pressure at the top of the reservoir is as high as the least principal stress in the overlying unit. In both cases, geomechanical characterization can be used to derive the pressures and rates of injection needed to reach those critical values and can therefore help in evaluating the potential risk of leakage.

Teapot Dome CO_2 EOR-carbon storage pilot

The Teapot Dome Field Experimental Facility (Fig. 1) is owned by the U.S. government and operated by the U.S. Department of Energy and the Rocky Mountain Oilfield Testing Center (RMOTC). This federal ownership assures a platform for long-term scientific investigations in a stable business context. The extensive data set of Teapot Dome is in the public domain, thus facilitating research of all kinds. These unique characteristics make Teapot Dome an ideal laboratory to conduct an EOR-Carbon Storage experiment in a mature oil reservoir. To evaluate the scientific and technical feasibility, the project team is working with interested industry and research partners to design the first CO_2 injection experiment, a small, short-duration EOR pilot, which would use existing wells and infrastructure. Project execution will be primarily contingent upon receiving adequate support from RMOTC's industry and research partners. The project envisioned would target the Tensleep Formation, with a minimum of $\sim$60 tons/day CO_2 for a minimum of $\sim$1.5 months.

Geology of Teapot Dome

Teapot Dome is an elongated asymmetrical, basement-cored anticline with a north-northwest axis. It is part of the Salt Creek structural trend (Fig. 1), located on the southwestern edge of the Powder River Basin (Cooper and Goodwin 1998; Beinkafner 1986). The anticline (Fig. 2) is interpreted as a west verging fault propagation fold, typical of many Laramide age folds in the Rocky Mountain Region (McCutcheon 2003; Milliken and Koepsell 2003). It is bounded on the west by a series of high-angle reverse faults of approximately 35–40° east-northeast dip (McCutcheon 2003). The anticline is compartmentalized into several blocks by major oblique strike-slip to normal faults (Fig. 2) involving the basement. In some cases these faults are actually a series of smaller faults, subparallel to a major fault. In cross-section they produce what is sometimes called a flower structure (Twiss and Moores 1992). These faults are well defined in the seismic data and in outcrops. In general they are oriented along a NE-SW trend, but vary in geometry, displacement and complexity. The major fault zones have been assigned arbitrary names S1, S2, S3 and S4 (McCutcheon 2003) as shown in Fig. 2.

The stratigraphy of Teapot Dome consists of Upper Cretaceous to Mississippian strata of diverse origin ranging from offshore sediments to coastal sandstone dunes over a granitic basement. The Tensleep Formation, of Pennsylvanian age, is the deepest hydrocarbon producing interval in the anticline. It contains multiple sequence boundaries in response to frequent and high-amplitude sea level changes (Zhang et al. 2005). In this area it consists of interdune deposits such as eolian sandstones, sabkha carbonates, evaporites (mostly anhydrite) and extensive beds of very low permeability dolomicrites. The average porosity is 10% (5–20% range), and the average permeability is 30 mD (10–100 mD range). The average net thickness is 15 m. The reservoir has a strong aquifer drive and therefore hydrostatic reservoir pressure, and the reservoir temperature is $\sim$88°C. The Tensleep Formation is divided into several intervals, of which the approximately 30 m thick B-Sandstone is the main producing horizon and the proposed storage interval for this experiment.

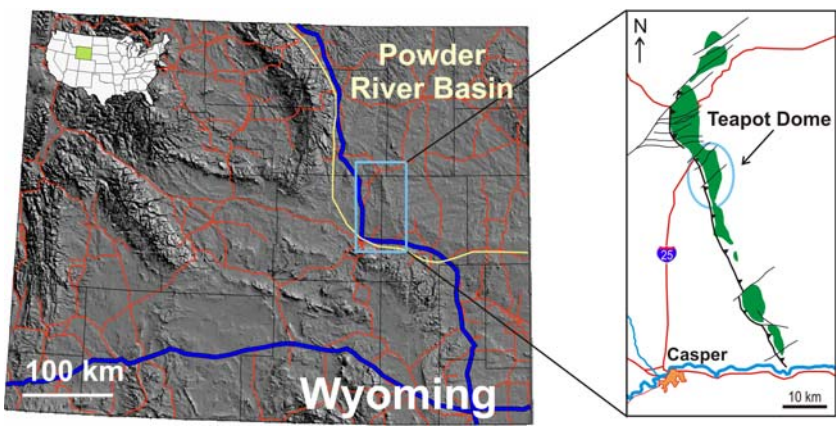

Fig. 1 Location of Teapot Dome. Satellite image of Wyoming (*left*), Salt Creek structural trend, topographic relief in *green* (*right*) (courtesy of RMOTC)

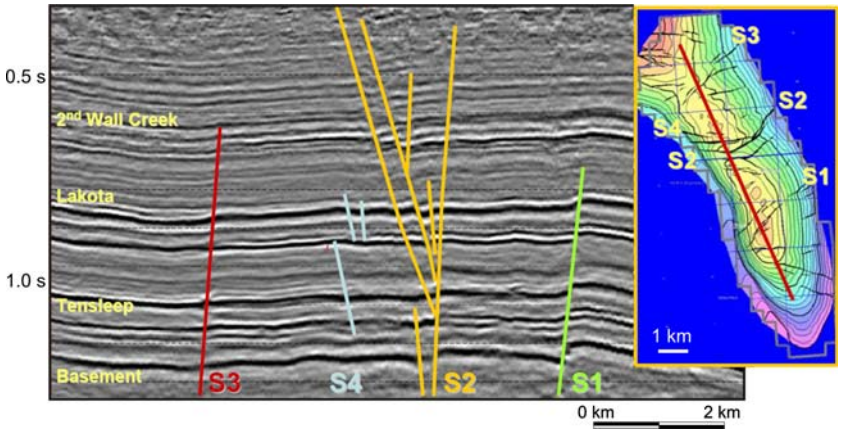

Fig. 2 NW-SE cross-section through Teapot Dome (*left*). Depth-structure map of 2nd Wall Creek Sandstone with locations of seismic line (*right*) (adapted from Friedmann et al. 2004)

The Opeche Shale plus the anhydrite of the Minnekahta Member of the Permian Goose Egg Formation (Fig. 4) comprise the regional seal of the Tensleep Formation throughout Wyoming. At the top of the Tensleep Formation there is a tightly cemented dolomitic eolian or interdune sandstone, with diagenetic effects possibly related to a long period of subaerial exposure. A major unconformity on this surface is characterized by a sedimentary breccia with clasts of the Tensleep Formation dolomitic sandstone suspended in a matrix of dolomitic and anhydritic sandstone of the Opeche Member. The 2-m thick Opeche Sandstone Member is capped by 17 m of redbed siltstone and sedimentary breccia of the Opeche Shale Member, deposited in an arid coastal plain setting. Overlying the Opeche Shale there are approximately 5 m of the Minnekahta Limestone, deposited in a carbonate shelf setting (M. D. Milliken, RMOTC, personal communication, 2006).

In the area under study the Tensleep Formation has its structural crest at 1,675 m below surface covering an area of approximately 1.2 km^2 (Fig. 3). The reservoir is trapped against a NE-SW trending fault to the north resulting in a three-way closure trap. A three-way trap is one in which the fluids are trapped by structural relief and the top seal on three sides of the trap, and by a sealing fault on the fourth side. The trapping fault, named S1, has been described as an oblique-slip basement-cored right-lateral tear fault (Milliken and Koepsell 2003). Figure 3 is a time-structure map of the Tensleep Formation. In a time-structure map the formation structure is mapped in two-way seismic travel time (TWTT) expressed in milliseconds, instead of depth/elevation. The red line, corresponding to the 1,050 ms contour, indicates the oil/water contact. There is approximately 40 ms TWTT of structural closure (approx. 100 m at velocity = 2,500 m/s), which is the vertical distance from the structural crest to the spill point of the structure on this reservoir. This means that around 100 m of fluid column height can be trapped.

Geomechanical characterization

To obtain the geomechanical model and perform a critically stressed fault analysis we follow the methodology of Zoback et al. (2003) for assessing the stress state and Wiprut and Zoback (2002) for assessing fault stability. The parameters needed for a full definition of the stress state are summarized in Table 1 along with the data sources used to constrain the parameters.

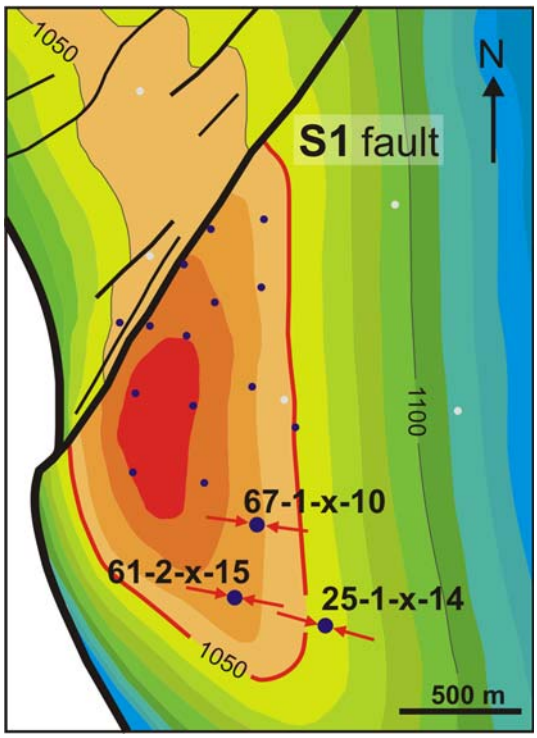

Fig. 3 Time-structure map in milliseconds of Tensleep Formation in Section 10 area showing the *S1 fault*, oil-contact area (*red contour line*), S_{Hmax} direction and analyzed wells (*blue dots*)

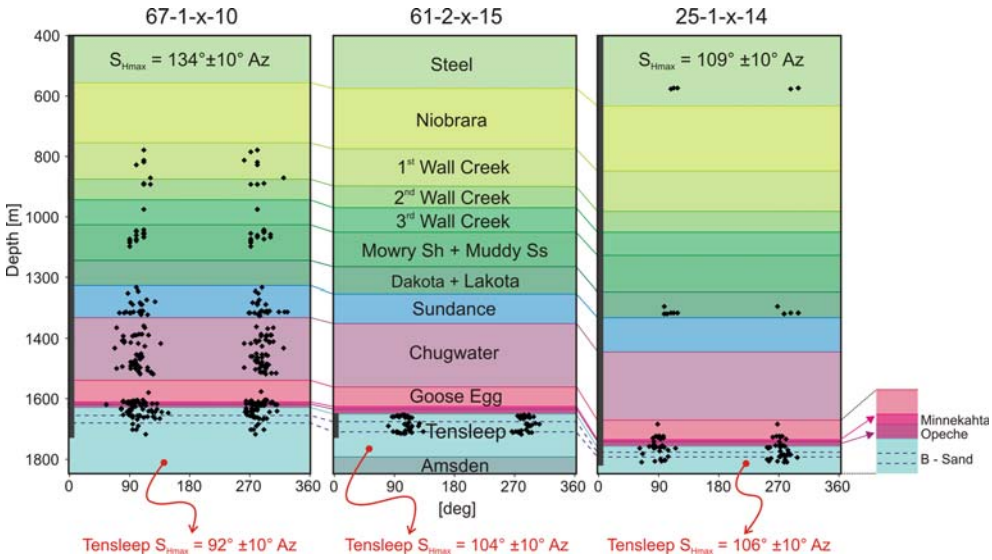

Fig. 4 Observations of drilling-induced tensile fractures in the three study wells. The orientation at the *top of each panel* indicates the average S_{Hmax} stress orientation from the entire interval studied. The stress orientation in the Tensleep Formation is indicated at the *bottom* of each figure. The *vertical bar* in each panel indicates the range of depths covered by the FMI log. The entire thickness of the Tensleep Formation is shown in the *middle panel*, but was not penetrated in the other two wells. The B sand is only ~30 m thick and located near the top of the formation

The magnitude of the vertical stress (S_v) is obtained by integration of rock densities taken from density logs from the surface to the depth of interest (see first row of Table 1 where z_0 is the depth of interest, ρ is the density and g is the gravity acceleration). Density logs measure the bulk density of the rocks in the wellbore walls through gamma ray emissions. The proportion of gamma rays emitted by the source and back-scattered to the detector depends on the electron density of the formation and therefore its matrix density (Jahn et al. 1998).

The least principal stress, S_3, which is usually the minimum horizontal principal stress (S_{hmin}), can be obtained from the analysis of hydraulic fracturing via either minifracs or extended leak-off tests after casing is set. Hydraulic fractures allow the determination of S_3 orientation and magnitude since they always propagate perpendicular to the least principal stress in the earth (Hubbert and Willis 1957).

While S_v and S_3 are relatively straightforward to estimate, the maximum horizontal stress (S_{Hmax}) magnitude can be obtained in different ways by modeling wellbore failure features such as drilling-induced tensile fractures (if S_v, S_{hmin} and pore pressure (P_p) values are known) or stress-induced wellbore breakouts (if S_v, S_{hmin}, P_p and the rock strength are known). The orientation of the horizontal principal stresses in vertical wells can be straightforwardly determined from wellbore failure orientations. Drilling-induced tensile fractures propagate parallel to S_{Hmax}, whereas breakouts form at the azimuth of S_{hmin}. Under normal drilling conditions, the occurrence of drilling-induced tensile fractures in a vertical well usually indicates a strike-slip faulting stress state (Zoback et al. 2003).

Density, sonic and Formation Microresistivity Imager (FMI) logs in the 67-1-*x*-10, 61-2-*x*-15 and 25-1-*x*-14 wells (see Fig. 3 for well locations) were analyzed to quantify the stress tensor (S_v, S_{Hmax} and S_{hmin}) in the area of interest. A sonic log measures the speed of sound in the wall of the borehole, and is related to both the porosity and lithology of the rock being measured, whereas the FMI log makes a detailed image of the rocks on all sides of the well hole by measuring resisitivity of the rock.

Table 1 Parameters and data needed to define the stress tensor and the geomechanical model

Parameter	Data
Vertical stress (S_v)	Density logs: $S_v(z_0) = \int_0^{z_0} \rho g dz$
Minimum horizontal stress (S_{hmin})	LOT, XLOT, minifrac
Maximum horizontal stress (S_{Hmax})	Modeling wellbore failures
Stress orientation	Orientation of wellbore failures
Pore pressure	Measure, sonic logs
Rock strength	Lab, logs, modeling well failure
Faults and fractures	Seismic, wellbore imaging

Stress orientation from FMI logs

Drilling-induced tensile fractures were analyzed in FMI logs from the three study wells. Interactive image analysis yielded 420 observations of drilling-induced tensile fractures over a depth range of 400–1,800 m (Fig. 4). The average maximum horizontal stress (S_{Hmax}) direction is 116 ± 15° AZ (N64°W). This value is consistent with the S_{Hmax} orientation of 105° AZ (N75°W), observed by Milliken and Koepsell (2003) in well 67-1-*x*-10. If we consider only the drilling-induced tensile fractures in the Tensleep Formation, the direction of S_{Hmax} is 100 ± 15° AZ (N80°W).

Figure 4 shows the distribution of tensile fractures and stratigraphic column on these wells. In well 67-1-*x*-10 tensile fractures are found through most of the column

while in well 25-1-*x*-14 there are surprisingly fewer features, even though the two wells were drilled with similar mud weights. In well 61-2-*x*-15 only part of the Tensleep Formation was imaged, where tensile fractures are present as well. Note the lack of breakouts at the depth of the Tensleep Formation.

The rock strength used in the horizontal stresses magnitude estimations was determined from sonic logs using an empirical relationship developed by Chang et al. (2006) for weak and unconsolidated sandstones in the Gulf Coast. The average estimated value of the B-Sandstone rock strength varies from 55 to 65 MPa in the three wells.

Figure 5 represents the range of allowable values for the horizontal principal stresses based on Coulomb faulting theory and Anderson's stress and faulting classifications system, provided depth, pore pressure and a particular coefficient of friction. The solid black line in Figure 5 outlines a polygon that defines the limits of Mohr–Coulomb failure for frictional equilibrium of pre-existing faults. The stress state must be inside of this polygon because the strength of the crust does not allow a larger stress difference between the greatest and least principal stresses. The black solid lines separate the three triangular regions reflecting normal faulting (NF), strike-slip faulting (SS) and reverse faulting (RF) stress conditions. NF implies $S_v = S_1 > S_{Hmax} = S_2 > S_{hmin} = S_3$, SS environment requires $S_{Hmax} = S_1 > S_v = S_2 > S_{hmin} = S_3$ whereas RF implies $S_{Hmax} = S_1 > S_{hmin} = S_2 > S_v = S_3$. The red contours on Fig. 5 discriminate the permissible stress states for a series of rock strengths whereas the blue contours delimit possible horizontal stress magnitudes based on the tensile strength of the rock (Moos and Zoback 1990; Zoback et al. 2003).

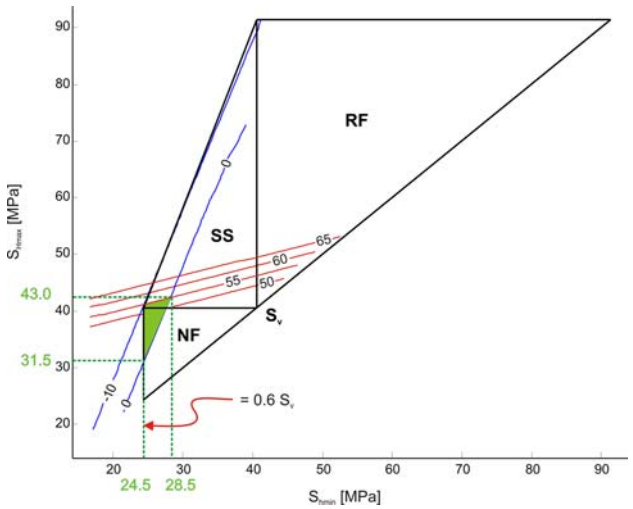

Fig. 5 Stress polygon for well 67-1-*x*-10 (see explanation in text) at depth = 1,656 m (top of Tensleep Formation), P_p = 16.56 MPa, S_v = 40.6 and compressive rock strength = 55 MPa. *Red lines* are isovalues of rock strength and *blue lines* represents isovalues of tensile rock strength

The magnitudes of S_{Hmax} and S_{hmin} were estimated from observed occurrence of drilling-induced tensile fractures and non-occurrence of wellbore breakouts, following Zoback et al. (2003). The green polygon in Fig. 5 shows the allowable magnitudes of S_{Hmax} and S_{hmin} for well 67-1-*x*-10 data at depth = 1,656 m (top of Tensleep Formation), hydrostatic P_p = 16.56 MPa, S_v = 40.6 and compressive rock strength (C) = 55 MPa. Since no breakouts were observed it was assumed that the calculated rock strength is the lower bound for the actual rock strength of the rock and acts as an upper bound for the S_{Hmax} magnitudes, as well as the zero tensile strength blue line. The mud weight and temperature, obtained from the drilling reports, were also considered and with these constraints the range of possible stress magnitudes was estimated. From the data in this particular well S_{Hmax} could range from 31.5 to 43.0 MPa and S_{hmin} from 24.5 to 28.5 MPa.

The analysis of the three studied wells yielded a NF/SS faulting stress state where $S_{Hmax} \approx S_v > S_{hmin}$. This is supported by fault movement observed in the youngest sections of the 3D seismic cube and by the displacements on NE/SW faults observed in the surface outcrops and trenches (Milliken 2005).

Due to the absence of leak-off or minifrac tests in the Tensleep Formation to obtain the magnitude of S_{hmin} (which would also better constrain the magnitude of S_{Hmax}), the critically stressed fault analysis was first performed with an S_{hmin} gradient of $0.6S_v$ and $S_{Hmax} = S_v$ expected for a NF/SS environment. Available data from a minifrac test performed in the 2nd Wall Creek reservoir confirms $S_{hmin} = 0.6S_v$. This minifrac test was performed in the well 71-1-*ax*-4, approximately 2 km northwest of the area under study, where the 2nd Wall Creek reservoir is at approximately 900 m depth and 720 m above the top of the Tensleep Formation.

With this information, a 2nd order stress tensor (S) that only varies with depth was defined as the base case scenario to estimate the leakage potential of the S1 fault. Since the present stress state corresponds to a NF/SS environment, $S_1 = S_{Hmax}$, $S_2 = S_v$ and $S_3 = S_{hmin}$ (see Eq. 1).

$$S = \begin{bmatrix} S_1 & 0 & 0 \\ 0 & S_2 & 0 \\ 0 & 0 & S_3 \end{bmatrix} = \begin{bmatrix} S_{Hmax} & 0 & 0 \\ 0 & S_v & 0 \\ 0 & 0 & S_{h\,min} \end{bmatrix} = \begin{bmatrix} S_v & 0 & 0 \\ 0 & S_v & 0 \\ 0 & 0 & 0.6S_v \end{bmatrix} \quad (1)$$

Fault slip potential using Coulomb criterion

The S1 fault was mapped in the available 3D seismic survey and converted to depth using the seismic dip

processing moveout velocities. To determine the risk of leakage through the S1 fault, the authors evaluated the state of stress and pore pressure acting on the fault plane following the methodology of Wiprut and Zoback (2002), which will be described below.

It is important to note that the orientation of the S1 fault has an azimuth of 36° which is nearly perpendicular to S_{Hmax} (see Fig. 3). Therefore it immediately appears unlikely that this fault could slip in a NF/SS stress field.

To perform the quantitative analysis, the shear (τ) and normal stresses (S_n) were calculated for each element of the fault. Then Coulomb failure criteria was applied to predict the critical pressure (P_c) necessary to reactivate fault slip, assuming a coefficient of friction (μ) of 0.6.

$$P_c = S_n - \tau/\mu. \quad (2)$$

Comparing this P_c with a reference P_p, modeled from the pressure data of the field, a critical pressure perturbation (P_{cp}) was obtained. P_{cp} indicates the pore pressure change to enable a fault element to slip given the stress state, fault orientation and reference P_p. In this analysis it is assumed that active faults are potential conduits for fluid migration such that P_{cp} indicates the leakage potential for each portion of the fault (Fig. 6a). It is important to note that this is a conservative approach for evaluating likelihood of CO_2 leakage along the fault, even though the amount of potential leakage could be quite small if the area of fault slip is small.

For the base case stress scenario defined in the previous section, at the depth of the Tensleep Formation (red line in Fig. 6a), approximately 17 MPa of excess pressure would be required to cause the fault to slip. This corresponds to a CO_2 column height of approximately 2,500 m (at a density of 700 kg/m^3). Since the average closure of the Tensleep Formation in this area is no more than 100 m, it is anticipated that the S1 fault is not at risk of reactivation and therefore will not be a leakage pathway for CO_2 migration.

To evaluate how poro-elastic effects affect fault stability, Eq. 3 was incorporated in the previous analysis. This equation was derived for an isotropic, porous and elastic reservoir that is infinite in extent. Segall and Fitzgerald (1996) showed that this relationship is also valid if the ratio of lateral extent to thickness of a reservoir is greater than 10:1 (which is the present case).

$$\Delta S_{Hor} = \alpha \frac{(1-2\nu)}{(1-\nu)} \Delta P_p \quad (3)$$

S_{Hor} corresponds to both S_{Hmax} and S_{hmin}, α is Biot's coefficient and ν is Poisson's ratio (Brown et al. 1994).

P_{cp} was estimated for a potential CO_2 injection-induced increase in P_p = 10 MPa, α = 1 and ν = 0.25. As it is shown in Fig. 6b, the poro-elastic effects increase the amount of extra pressure needed to cause slip in the S1 fault. At the depth of the Tensleep Formation (red line in Fig. 6b) approximately 20 MPa of excess pressure would be required.

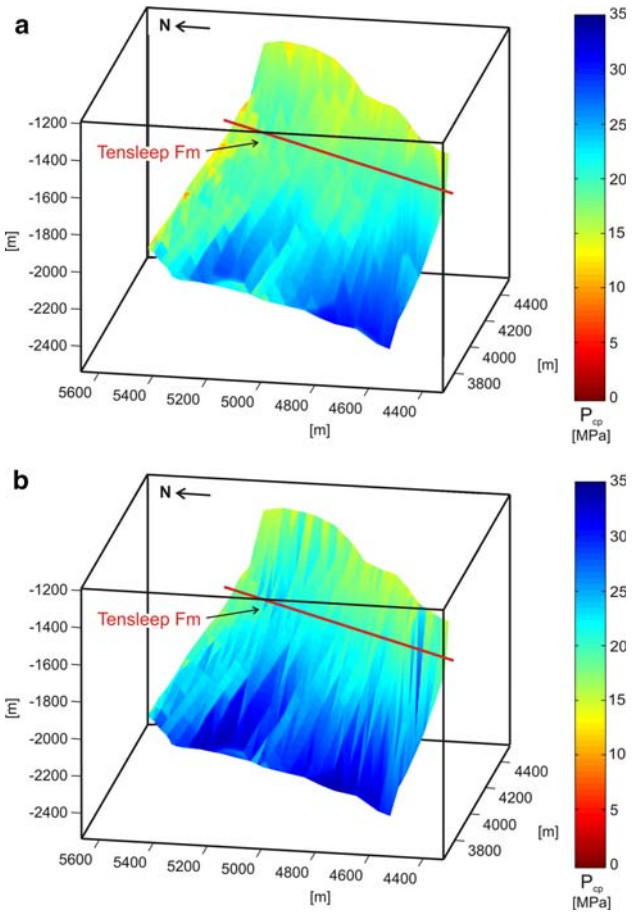

Fig. 6 **a** Fault surface color-coded with critical pressure perturbation values indicating the fault slip potential. At the Tensleep Formation (*red line*), ~17 MPa of excess pressure would be required to cause the fault to slip. **b** Fault surface color-coded with critical pressure perturbation values indicating the fault slip potential considering the poro-elastic effect. At the Tensleep Formation (*red line*), ~20 MPa of excess pressure would be required to cause the fault to slip

Critical pressure perturbation sensitivity analysis

To evaluate how the uncertainties in the horizontal stress magnitudes and in the strike and dip of the fault with respect to the stress field affect the slip potential of the S1 fault, a sensitivity analysis of those parameters was performed. In the case of the fault orientation we need to account for the limits in the seismic resolution as well as for the uncertainties in the time-depth conversion of the structures mapped. During the seismic acquisition, the

travel time of a wave from the surface to the objective at depth is measured. To convert the measured travel time to depth it is necessary to assume the velocity of the wave, from which comes the uncertainty on real depths and geometry of the bodies under consideration.

Random distributions of the components of the stress tensor were generated based on the mean, minimum and maximum stress values estimated for each well. For the base cases of a normal fault ($S_1 = S_v$, $S_2 = S_{Hmax}$ and $S_3 = S_{hmin}$) and strike-slip ($S_1 = S_{Hmax}$, $S_2 = S_v$ and $S_3 = S_{hmin}$), cases were analyzed separately using over 10,000 Monte Carlo Simulations. In the case of normal faulting, S_{Hmax} is less than S_v and greater than S_{hmin}. In the strike-slip case, S_v is less than S_{Hmax} and greater than S_{hmin}. Figures 7 (for normal faulting) and 8 (for strike-slip faulting) show the fault slip potential probability as a function of reservoir pressure for variations of the indicated component of the stress tensor (while the others remained fixed). From this analysis it was established that in 99.9% of the cases a pressure perturbation of more than 10 MPa would be necessary to induce slip on the S1 fault.

To account for the uncertainties with respect to the geometry of the fault, Fig. 9 evaluates fault slip probability as a function of variations in fault azimuth (Fig. 9 left) and dip (Fig. 9 right). These cases were evaluated with the mean values of the stress tensor. The dip angle has the biggest impact on the fault slip potential. In 99.9% of the test scenarios, the critical pressure perturbation values are above 10 MPa.

Even in the most pessimistic risk scenario, a CO_2 column height of approximately 1,500 m (using a reasonable average density $\sim$700 kg/m^3) is required to reach the lowest estimated P_{cp} value ($\sim$10 MPa).

Hydraulic fracture limit for caprock

Better constraints on the least principal stress (S_{hmin}) in both the reservoir and the caprock are necessary not only to more precisely estimate the magnitudes of S_{hmin} and S_{Hmax}, but also to get more exact values for the maximum pressure increase at the top of the structure that the reservoir could sustain before hydrofracturing the overlying unit.

Knowledge on the hydraulic fracture limit of the caprock is important for two reasons. It is useful for evaluating the risk of leakage, and it provides a constraint on the maximum CO_2 column height that the reservoir can contain if hydraulic fracturing of the overlying unit occurs before the column reaches the spill point of the structure. In other words, the hydraulic fracture limit helps to evaluate whether there is a dynamic constraint for the CO_2 column in the area under study (e.g., Finkbeiner et al. 2001).

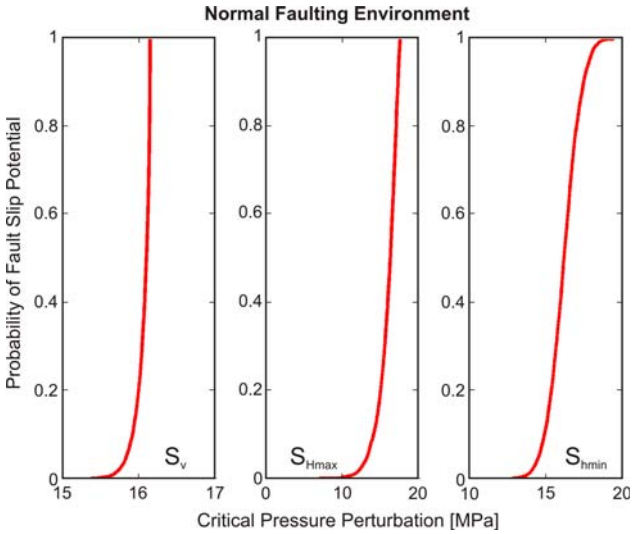

Fig. 7 Fault slip potential probability for Normal Fault environment, as a function of each of the components of the stress tensor, varying S_v (maintaining S_{Hmax} = 34.4 MPa and S_{hmin} = 25.7 MPa fixed) (*left*); varying S_{Hmax} (maintaining S_v = 39.9 MPa and S_{hmin} = 25.7 MPa fixed) (*center*) and varying S_{hmin} (maintaining S_v = 39.9 MPa and S_{Hmax} = 34.4 MPa fixed) (*right*)

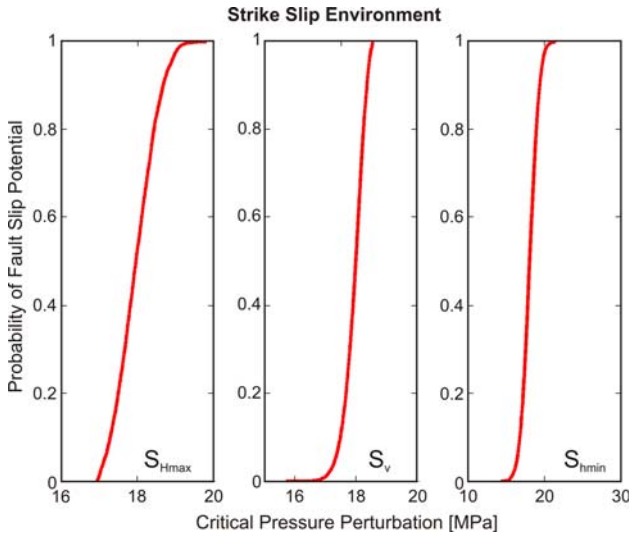

Fig. 8 Fault slip potential probability for Strike-Slip environment, as a function of each of the components of the stress tensor, varying S_{Hmax} (maintaining S_v = 39.6 MPa and S_{hmin} = 25.7 MPa fixed) (*left*); varying S_v (maintaining S_{Hmax} = 45.5 MPa and S_{hmin} = 25.7 MPa fixed) (*center*) and varying S_{hmin} (maintaining S_{Hmax} = 45.5 MPa and S_v = 39.6 MPa fixed) (*right*)

In order to better estimate the value of S_{hmin}, we need either a leak-off test or minifrac in the caprock. In the drilling reports of the three studied wells, no fluid loss information was recorded and no leak-off test or minifrac test data are available at Teapot Dome, other than the one mentioned in the 2nd Wall Creek reservoir.

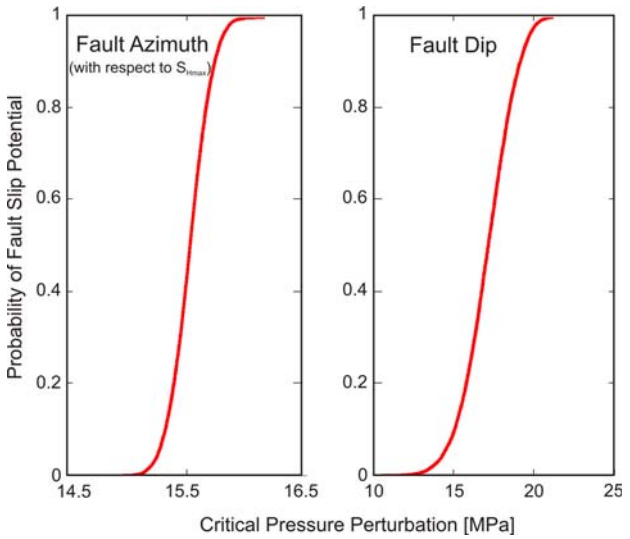

Fig. 9 Fault slip potential probability as function of variation in the fault azimuth (*left*) and in the fault dip angle (*right*). The mean value of the stress tensor (S_v = 39.90, S_{Hmax} = 34.40 and S_{hmin} = 25.72 MPa) was used to analyze these scenarios

With the better constrained value of S_{hmin}, it will be possible to evaluate whether the hydrofracture limit of the Tensleep Formation or the caprock could be a lower constraint in the sustainable injection pressure than the estimated P_{cp} on the fault.

Conclusions

A comprehensive geomechanical model for the Tensleep Formation was generated in the context of providing the technical foundation required for RMOTC and its partners to consider and design a CO_2 injection project at Teapot Dome. This model allows the project team to quantitatively estimate the pore pressure at which the S1 fault would slip, and therefore supports predictions about the risk of leakage in the target storage unit.

The components of the stress tensor as well as the geometry of the fault were considered in a probabilistic sensitivity analysis, from which it was established that for even the most pessimistic scenario (lower values of fault dip), 99.9% of the cases would require at least 10 MPa of excess pressure to cause the S1 fault to reactivate. This pressure would be seen at the top of a CO_2 column of approximately 1,500 m in height. As the average closure of the Tensleep Formation structure in this area does not exceed 100 m, the S1 fault does not appear to be at risk of reactivation and therefore providing a leakage pathway for CO_2 under the present stress field.

Planned refinements to this analysis are direct measurements of S_{hmin} in the Tensleep Formation as well as in the caprock. These data will provide more reliable estimates for the maximum sustainable pressure before hydrofracturing the caprock, as well as for the maximum CO_2 column height that this structure could support. The sensitivity analysis highlighted the influence of the fault dip angle in the P_{cp} estimation. Thus refining the time-depth conversion model to accurately estimate the dip of the fault is also essential. The possible presence of faults with smaller displacements than the one detectable by the seismic (but potentially more favorable orientations for reactivation) will have to be evaluated. These can be observed either in FMI fracture interpretations and well correlation, or from surface reservoir analogs at Tensleep Formation outcrops, which could have the same deformation style present in the subsurface.

Acknowledgments The authors would like to acknowledge the Global Climate and Energy Project (GCEP) for funding the present research, as well as Brian Black, Tom Anderson and Mark Milliken from RMOTC, Tapan Mukerji, Kyle Spikes and Amie Lucier from Stanford University, and Tim McCutcheon from McCutcheon Energy. Additionally the authors would like to acknowledge GMI for providing some of the software used in the present research.

References

Beinkafner K (1986) Use of dipmiter logs to refine structural mapping of Teapot Dome, Wyoming. AAPG Bull 70(8):1031

Brown KM, Bekins B, Clennell B, Dewhurst D, Westbrook GK (1994) Heterogeneous hydrofracture development and accretionary fault dynamics. Geology (22):259–262

Chang C, Zoback MD, Khaksar A (2006) Empirical relations between rock strength and physical properties in sedimentary rocks. J Petrol Sci Eng 51:223–237

Cooper SP, Goodwin LB (1998) Fracture characterization and variability within a basement-cored Laramide age anticline, Teapot Dome, Wyoming. AAPG Annual Convention Extended Abstract #A132, vol.1, 1p. Teapot Dome (WY)

Finkbeiner T, Zoback MD, Flemings P, Stump B (2001) Stress, pore pressure, and dynamically constrained hydrocarbon columns in the South Eugene Island 330 Field, northern Gulf of Mexico. Am Assoc Petrol Geol 85(6):1007–1031

Friedmann SJ, Nummedal D, Stamp VW (2004) Science and technology goals of the Teapot Dome field experimental facility. NETL 3rd annual carbon sequestration conference proceedings. Exchange Monitor Publications, Alexandria

Grasso JR (1992) Mechanics of seismic instabilities induced by the recovery of hydrocarbon. Pure Appl Geophys 139(3/4):507–533

Hubbert MK, Willis DG (1957) Mechanics of hydraulic fracturing. Pet Trans AIME 210:153–163

Jahn F, Cook M, Graham M (1998) Hydrocarbon exploration and production. Elsevier, Amsterdam, 384pp

McCutcheon T (2003) Time structure maps–3D seismic data interpretation, Teapot Dome Oil Field, Naval Petroleum Reserve No. 3, Natrona County, Wyoming. Rocky Mountain Oilfield testing center report

Milliken MD (2005) Surface mapping validates 3D seismic faulting interpretations at Teapot Dome Field, Natrona Co., Wyoming. http://www.searchanddiscovery.com/documents/abstracts/2005rocky/RMmilli.htm

Milliken MD, Koepsell R (2003) Imaging technology offers enhanced interpretatio of Teapot Dome reservoirs. Geological Association. 2002 field conference: "Wyoming Basins" and 2003 field conference. Casper, Wyoming, pp 41–62

Moos D, Zoback MD (1990) Utilization of observations of well bore failure to constrain the orientation and magnitude of crustal stresses: application to continental, deep sea drilling project and ocean drilling program boreholes. J Geophys Res 95(B6):9305–9325

Raleigh CB, Healy JH, Bredehofft JD (1976) An experiment in earthquake control at Rangeley, Colorado. Science 191:1230–1237

Segall P, Fitzgerald SD (1996) A note on induced stress changes in hydrocarbon and geothermal reservoirs. Tectonophysics 289:117–128

Twiss RJ, Moores EM (1992) Structural geology. W.H. Freeman, New York, 532pp

Wiprut DJ, Zoback MD (2002) Fault reactivation, leakage potential, and hydrocarbon column heights in the northern North Sea. In: Koestler AG, Hunsdale R (eds) Hydrocarbon seal quantification, vol 11. NPF Special Publication, Elsevier, Amsterdam, pp 203–219

Zhang Q, Nummedal D, Yin P (2005) Stratigraphy, sedimentology and petrophysics of the Tensleep Sandstone at Teapot Dome and in outcrop. http://www.searchanddiscovery.com/documents/abstracts/2005rocky/RMzha.htm

Zoback MD, Barton CA, Brudy M, Castillo DA, Finkbeiner T, Grollimund BR, Moos DB, Peska P, Ward CD, Wiprut DJ (2003) Determination of stress orientation and magnitude in deep wells. Int J Rock Mechan Mining Sci 40:1049–1076